Table IV. *Effect of various dosage levels of E_2 on number of mammary carcinoma per rats without corpora lutea.*

Group	Number of rats examined	Number of rats with mammary carcinomas and no corpora lutea Number of mammary carcinomas/rats without corpora lutea Day of mass detection ~50[a]	~100[a]	~150[a]	~200[a]	~250[a]
17β-estradiol 0.1 μg/body	3	0 (0%) –	1 (33%) 0.3±0.6	2 (67%) 1.3±1.5	2 (67%) 1.3±1.5	3 (100%) 2.7±2.9
17β-estradiol 1 μg/body	3	0 (0%) –	0 (0%) –	1 (33%) 0.3±0.6	1 (33%) 0.3±0.6	3 (100%) 3.0±1.0
17β-estradiol 10 μg/body	7	0 (0%) –	2 (29%) 0.3±0.5	2 (29%) 0.3±0.5	5 (71%) 0.7±0.5	6 (86%) 1.6±1.3
17β-estradiol 100 μg/body	9	0 (0%) –	1 (11%) 0.1±0.3	2 (22%) 0.3±0.7	4 (44%) 0.7±0.9	7 (78%) 1.4±1.0
17β-estradiol 1000 μg/body	12	0 (0%) –	0 (0%) –	2/ (17%) 0.2±0.4[b]	3 (25%) 0.3±0.7	3 (25%) 0.3±0.7[b]

[a]Days after birth (approximately days)
[b]$p<0.05$: significantly different from the 0.1 μg/body group
–: not detected

Table V. *Effects of various dosage levels of E_2 on incidence of rats with corpora lutea, and ovary weights.*

Group	Number of rats examined for corpora lutea	Number of rats with corpora lutea	Number of rats for which the ovaries were weighed	Ovary weight (g)/group Mean±SD
Control	21	21 (100%)	14[a]	0.122±0.032
17β-estradiol 0.1 μg/body	14	11 (79%)[b]	14	0.105±0.013
17β-estradiol 1 μg/body	15	12 (80%)[b]	15	0.140±0.029
17β-estradiol 10 μg/body	27	20 (74%)[b]	25[a]	0.128±0.038
17β-estradiol 100 μg/body	20	11 (55%)[c]	20	0.099±0.033
17β-estradiol 1000 μg/body	12	0 (0%)[c]	12	0.058±0.045[c]

[a]Organ weights of animals that died were not weighed
[b]$p<0.05$: significantly different from the control group
[c]$p<0.01$: significantly different from the control group

Table VI. *Effect of various dosage levels of E_2 on the number of terminal end buds (TEBs), and the number of rats with corpora lutea at age of 50 days.*

Group	Number of rats examined	Number of TEBs/rat (Mean±SD)	Rats with corpora lutea
Control	10	46.0±4.6	10 (100%)
17β-estradiol 0.1 μg/body	9	47.3±8.2	9 (100%)
17β-estradiol 1 μg/body	9	42.3±8.4	8 (100%)
17β-estradiol 10 μg/body	10	54.3±9.2[a]	10 (100%)
17β-estradiol 100 μg/body	10	41.0±11.9	10 (100%)
17β-estradiol 1000 μg/body	8	11.8±9.0[b]	0 (0%)[b]

[a]$p<0.05$: significantly different from the control group
[b]$p<0.01$: significantly different from the control group

days; therefore, it was considered that not only a physiological volume of estrogen, but also progesterone, may have been present at the time of carcinogenic exposure to DMBA. It is possible that the progesterone remained for some time during the progression period, resulting in mammary carcinomas that progressed to tumors.

The number of TEBs in the E_2-dosed groups during the neonatal period decreased significantly in the 1000 μg group and increased significantly in the 10 μg group at the age of 50 days. TEBs, undifferentiated terminal ductal structures with a multilayer of highly proliferative epithelial cells, are extremely vulnerable to chemical carcinogenesis (12). The incidence of carcinomas in rodents is directly associated with the density of TEBs in mammary glands at the time of carcinogen administration (12, 13). In response to stimulation from the mammogenic hormones, TEBs differentiate to the more mature structures, namely, alveolar buds (ABs) and lobules

(LOBs), which are less susceptible to carcinogens (12, 14). The progressive differentiation of TEBs into ABs is accentuated by the estrous cycle, which begins at the age of 30-42 days. Development of the mammary gland in non-pregnant females is strongly controlled by the ovary. Ovariectomy can cause regression of the end buds and cessation of growth (15). Since TEBs are considered to be located in the region of the mammary gland most sensitive to DMBA (16, 17), the decreased incidence of mammary carcinomas in the 1000 μg group was thought to have resulted from the decreased number of TEBs seen in this group. A decrease in the number of TEBs noted in the 1000 μg group resulted from rapid differentiation of the mammary glands due to a high dosage of E_2 (unpublished data). The increase in mammary carcinomas noted in the 10 μg group is thought to have been due to increases in the number of TEBs seen in this group, since it is known that the incidence of mammary carcinomas positively correlates with the number of TEBs in the mammary glands of young nulliparous rats at the time of carcinogen exposure (12).

In conclusion, it is suggested that neonatal administration of E_2 affects the gonadotropin-secreting system, resulting in a change in the endocrine system which is thought to influence the progression of mammary carcinomas induced by DMBA. Moreover, neonatal administration of E_2 directly affects the mammary glands, and it is suggested that E_2 may promote the differentiation of TEBs, resulting in inhibitory effects on the initiation of mammary carcinomas. From these results, it is considered necessary that the effects of estrogenic chemicals, such as endocrine-disrupting chemicals, during the neonatal period on the development of mammary carcinomas be further investigated.

Acknowledgements

We are grateful to Mr. T. Kodama, Ms. N. Shirasaka, Ms. Y. Jitoho and Mr. G. Martin for their technical assistance. This work was supported in parts by the Kodama Fund for Medical Research, Japan.

References

1 Yoshida H, Ohi Y, Takasaki T, Kuriwaki K, Honda H, Sato E, Tanaka S, Tokunaga M, Nakamura T and Yoshida N: Sharp increase in the incidence of mammary carcinoma in Kagoshima Prefecture, Japan. Breast Cancer *3*: 9-12, 1996.
2 Martin FL: Genotoxins and the initiation of sporadic breast cancer. Mutagenesis *16*: 155-161, 2001.
3 Wright T and McGechan A: Breast cancer: new technologies for risk assessment and diagnosis. Mol Diagn *7*: 49-55, 2003.
4 Willoughby KN, Sarkar AJ, Boyadjieva NI and Sarkar DK: Neonatally administered tert-octylphenol affects onset of puberty and reproductive development in female rats. Endocrine *26*: 161-168, 2005.
5 Massart F, Seppia P, Pardi D, Lucchesi S, Meossi C, Gagliardi L, Liguori R, Fiore L, Federico G and Saggese G: High incidence of central precocious puberty in a bounded geographic area of northwest Tuscany: an estrogen disrupter epidemic? Gynecol Endocrinol *20*: 92-98, 2005.
6 Safe S: Clinical correlates of environmental endocrine disruptors. Trends Endocrinol Metab *16*: 139-144, 2005.
7 Yoshida H and Fukunishi R: Effect of neonatal administration of sex steroids on 7, 12-dimethylbenz[*a*]anthracene-induced mammary carcinoma and dysplasia in female Sprague-Dawley rats. Gann *69*: 627-631, 1978.
8 Yoshida H, Kadota A, Fukunishi R and Matsumoto K: Induction of mammary dysplasia and mammary carcinoma in neonatally androgenized female rats by 7, 12-dimethylbenz[*a*]anthracene. J Natl Cancer Inst *64*: 1105-1112, 1980.
9 Yoshida H, Fukunishi R, Kato Y and Matsumoto K: Progesterone-stimulated growth of mammary carcinomas induced by 7, 12-dimethylbenz[*a*]anthracene in neonatally androgenized rats. J Natl Cancer Inst *65*: 823-828, 1980.
10 Yoshida H and Huggins C: Effects of neonatally administered-testosterone propionate on the development of target organs of sex hormones and the induction of mammary carcinomas by 7, 8, 12-trimethylbenz (α) anthracene in female Sprague-Dawley rats. Exp Anim *30*: 303-305, 1981.
11 Yoshida H, Kodama A and Fukunishi R: Pathology of early lesions of mammary carcinoma and mammary dysplasia induced by 7, 12-dimethylbenz[*a*]anthracene in neonatally androgenized Sprague-Dawley female rats. Virchows Arch B Cell Path *34*: 33-41, 1980.
12 Russo J and Russo IH: DNA labeling index and structure of the rat mammary gland as determinants of susceptibility to carcinogenesis. J Natl Cancer Inst *61*: 1451-1495, 1978.
13 Russo J, Wilgus G and Russo IH: Susceptibility of the mammary gland to carcinogenesis: differentiation of the mammary gland as determination of tumor incidence and type of lesion. Am J Pathol *96*: 721-736, 1979.
14 Russo J and Russo IH: Biology of disease: biological and molecular bases of mammary carcinogenesis. Lab Invest *57*: 112-137, 1987.
15 Russo IH and Russo J: Mammary gland neoplasia in long-term rodent studies. Environm Health Perspect *104*: 938-967, 1996.
16 Shilkaitis A, Green A, Steele V, Lubet R, Kelloff G and Christov K: Neoplastic transformation of mammary epithelial cells in rats is associated with decreased apoptic cell death. Carcinogenesis *21*: 227-233, 2000.
17 Rowlands JC, Hakkak R, Martin J, Ronin J and Badger TM: Altered mammary gland differentiation and progesterone receptor expression in rats fed soy and whey proteins. Toxicolog Sci *70*: 40-45, 2002.

Received September 28, 2005
Accepted November 14, 2005

CASE REPORT

"End-Stage Kidney" in Longstanding Bulimia Nervosa

Daisuke Yasuhara, MD[1]*
Tetsuro Naruo, MD, PhD[1]
Shuhei Taguchi, MD, PhD[2]
Yoshihisa Umekita, MD, PhD[2]
Hiroki Yoshida, MD, PhD[2]
Shin-ichi Nozoe, MD, PhD[3]

ABSTRACT

Objective: The extent of renal damage over long-term binge/purges has not been well documented in bulimia nervosa (BN).

Method: We describe a 52-year-old woman with longstanding BN subsequent to an 8-year history of anorexia nervosa (AN).

Results: The patient showed chaotic binge/purges and chronic severe hypokalemia after recovery from AN at age 26 years, and renal biopsy showed juxtaglomerular hyperplasia, which was diagnosed as pseudo-Bartter's syndrome. Over the following 26 years, the patient's eating behaviors remained chaotic, and her renal function gradually deteriorated. After the patient died of pneumonia and sepsis at age 52 years, autopsy of her kidney showed chronic interstitial nephritis, proximal tubular swelling, and diffuse glomerular sclerosis, suggesting chronic glomerular injury associated with long-term binge/purges.

Conclusion: To our knowledge, this is the first case report of a patient with BN with long-term binge/purges who developed an eventual "end-stage kidney" characterized by hypokalemic nephropathy and diffuse glomerulosclerosis.

(Int J Eat Disord 2005; 38:383–385)

Introduction

Eating disorders, including anorexia nervosa and bulimia nervosa, are commonly seen in adolescents and young females. Particularly for bulimia nervosa, the increasing prevalence rate (1%–2% in 16–35-year-old females) and chronicity after treatment can result in serious social and medical problems (Fairburn & Harrison, 2003; Fairburn, Cooper, Doll, Norman, & O'Connor, 2000). Many medical complications associated with abnormal eating habits exist, including disturbances in gastrointestinal, metabolic, endocrine, and renal function (Fairburn & Harrison, 2003). In particular, renal function has been reported to be impaired even in the short term by severe energy restriction in anorexia nervosa, and by binge/purges in bulimia nervosa (Bock, Cremer, & Werner, 1978; Copeland, 1994; Riemenschneider & Bohle, 1983; Ishikawa et al., 1999; Sharp & Freeman, 1993; Tsuchiya, Nakauchi, Hondo, & Nihei, 1995;). However, little is known about the extent of renal damage over long-term binge/purges. We describe a patient with bulimia nervosa who suffered from longstanding binge/purges and eventual characteristic morphologic changes in her kidney.

Accepted 20 December 2004
Supported by a research grant from the Japanese Ministry of Health, Labor and Welfare.
Correspondence to: Daisuke Yasuhara, MD, Department of Behavioral Medicine, Kagoshima University Graduate School of Medical and Dental Science, 8-35-1 Sakuragaoka, Kagoshima-City 890-8520, Japan. E-mail: yasuhara@m3.kufm.kagoshima-u.ac.jp
[1] Department of Behavioral Medicine, Kagoshima University Graduate School of Medical and Dental Science, Kagoshima-City, Japan
[2] Department of Tumor Pathology, Course for Advanced Therapeutics, Graduate School of Medical and Dental Science, Kagoshima University, Kagoshima-City, Japan
[3] Department of Clinical Psychology, Faculty of Human Studies, Shigakukan University, Kagoshima, Japan
Published online 17 October in Wiley InterScience (www.interscience.wiley.com). DOI: 10.1002/eat.20198

Case Report

A 26-year-old woman was admitted to our hospital with general fatigue and severe emaciation (body mass index [BMI], 12.8 kg/m^2) in 1975. The patient had no personal history of physical disorders (e.g., diabetes mellitus, hypertension, or renal disease) but she had an 8-year history of anorexia nervosa, binge/purge type (American Psychiatric Association [APA], 1994). On examination, the patient displayed severe hypokalemia (2.0 mmol/L), anemia (hemoglobin level, 7.0 g/dl), and a total protein level of 5.8 g/dl. Blood urea nitrogen (BUN) and serum creatinine concentrations were within normal ranges (BUN level, 10.3 mg/dl; creatinine level, 0.9 mg/dl). However, her creatinine clearance was decreased (58 L/day). Renal biopsy showed no primary or secondary glomerular diseases, but juxtaglomerular hyperplasia, which was diagnosed as pseudo-Bartter's syndrome, was evident. Although

the patient regained weight (BMI, 18.4 kg/m^2) after intensive physical/psychological treatments for 6 months and abnormalities in laboratory studies except for hypokalemia (3.0 mmol/L) were normalized, her binge/purges were unstable and the patient developed bulimia nervosa, purging type (APA, 1994).

After discharge, although the patient maintained normal body weight (BMI > 18.0 kg/m^2) and worked at a local supermarket until age 39 years (1988), her binge/purges were still chaotic. At age 40 years (1989), the patient was referred to our hospital again because of general fatigue, and physical examinations revealed gastroenteritis, esophageal ulcer, hypokalemia (2.5 mmol/L), anemia (hemoglobin level, 8.0 g/dl), and renal insufficiency (BUN level, 46.8 mg/dl; creatinine level, 2.0 mg/dl). Although intensive treatments were applied and her general condition, except for hypokalemia and renal insufficiency, improved, her binge/purges were resistant to treatment and renal impairment gradually worsened (BUN level, 68.0 mg/dl; creatinine level, 5.0 mg/dl, in 1998).

The patient died of pneumonia and sepsis at age 52 years (2001), and autopsy showed bronchopneumonia, gastroenteritis, esophageal ulcer, and bilateral atrophic kidney with multiple cysts (Figure 1). Microscopic examination of the kidney (Figure 2) showed interstitial nephritis (e.g., lymphocytic cellular infiltration), proximal tubular swelling, and diffuse glomerular sclerosis (e.g., atrophy and hyalinized glomeruli). There were no findings relevant to primary or secondary glomerular diseases or juxtaglomerular hyperplasia.

Conclusion

Abnormal eating habits (e.g., severe energy restriction or compensatory binge/purges) have been previously reported to cause renal insufficiency in bulimia nervosa, but were not severe enough to require hemodialysis (Copeland, 1994). However, few studies have revealed the extent of renal damage, especially morphologic changes, over long-term bulimic symptoms (Bock et al., 1978; Copeland, 1994; Riemenschneider & Bohle, 1983; Tsuchiya et al., 1995). To our knowledge, this is the first case report of a patient with longstanding bulimia nervosa and an eventual "end-stage kidney" characterized by hypokalemic nephropathy and diffuse glomerulosclerosis.

Renal insufficiency in eating disorders has been reported to be induced by hypokalemia relevant to vomiting or laxative abuse (Bock et al., 1978; Copeland, 1994; Ishikawa et al., 1999; Riemenschneider & Bohle, 1983; Tsuchiya et al., 1995). The initial biopsy (1977) showed juxtaglomerular hyperplasia, and repeated biopsy (2001) showed interstitial nephritis and proximal tubular swelling. We deem that these morphologic changes were consistent with previous research on hypokalemic nephropathy (Bock et al., 1978; Copeland, 1994; Ishikawa et al., 1999; Riemenschneider & Bohle, 1983; Tsuchiya et al., 1995), and that hypokalemia played an important role in the long-term progress of renal insufficiency in this patient.

Glomerular sclerosis, as seen in our case, appeared to be induced by increased glomerular capillary pressure, glomerular hypertrophy, renal ischemia, and other poorly identified factors relevant to glomerular injury (Marcussen, 1992; Rennke, 1988). In addition to hypokalemia (Bock

FIGURE 1. Bilateral atrophic kidney with multiple cysts.

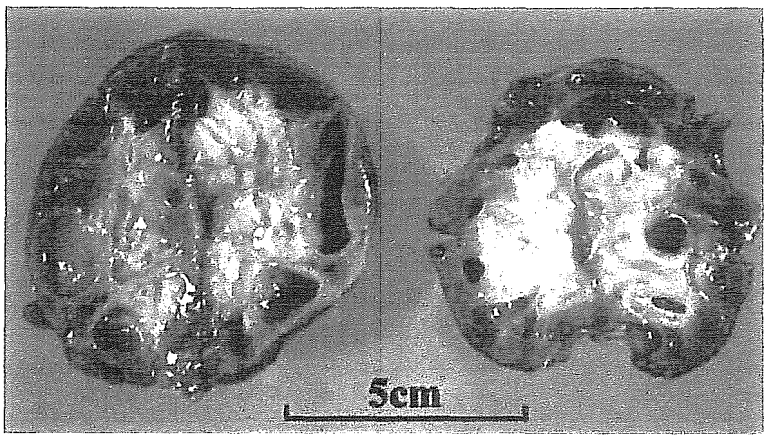

FIGURE 2. (A) Interstitial nephritis and diffuse glomerulosclerosis. (B) Proximal tubular swelling (arrows).

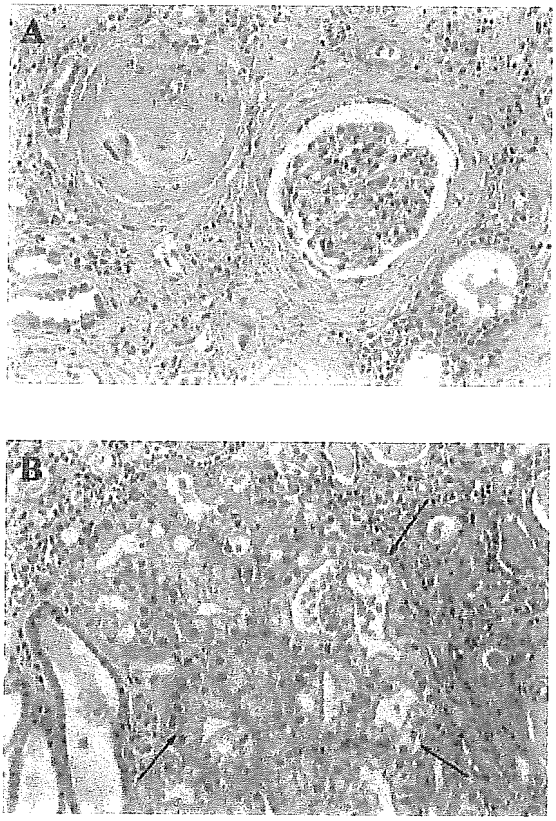

et al., 1978; Copeland, 1994; Ishikawa et al., 1999; Riemenschneider & Bohle, 1983; Tsuchiya et al., 1995), renal insufficiency might be induced by volume depletion relevant to severe energy restriction, vomiting, and laxative abuse in eating disorders (Copeland, 1994). Therefore, we deem that chronic glomerular injury induced by hypokalemia and volume depletion might have resulted in glomerular sclerosis in our patient. Further studies of a larger sample population are needed to investigate the pathogenesis of progressive glomerulosclerosis in bulimia nervosa.

Although physical complications of eating disorders are common, clinicians tend to overlook them (Sharp & Freeman, 1993). Although renal dysfunction in anorexia nervosa appears to be normalized after weight restoration (Boag, Weerakoon, Ginsburg, Havard, & Dandona, 1985), habitual binge/purges in bulimia nervosa tend to be treatment resistant and longstanding (Fairburn & Harrison, 2003; Fairburn et al., 2000), which could lead to irreversible renal changes, as seen in this case. Therefore, our case stresses the importance of early detection, adequate treatment, and intensive monitoring of the physical condition of a patient with bulimia nervosa. Clinicians and bulimic patients themselves should keep in mind the consequences associated with long-term habitual binge/purges.

References

American Psychiatric Association. (1994). Diagnostic and statistical manual of mental disorders (4th ed.). Washington, DC: Author.

Boag, F., Weerakoon, J., Ginsburg, J., Havard, C.W., & Dandona, P. (1985). Diminished creatinine clearance in anorexia nervosa: Reversal with weight gain. Journal of Clinical Pathology, 38(1), 60–63.

Bock, K.D., Cremer, W., & Werner, U. (1978). Chronic hypokalemic nephropathy: A clinical study. Klinische Wochenschrift, 56(Suppl.1), 91–96.

Copeland, P.M. (1994). Renal failure associated with laxative abuse. Psychotherapy and Psychosomatics, 62(3–4), 200–202.

Fairburn, C.G., Cooper, Z., Doll, H.A., Norman, P., & O'Connor, M. (2000). The natural course of bulimia nervosa and binge eating disorder in young women. Archives of General Psychiatry, 57, 659–665.

Fairburn, C.G., & Harrison, P.J. (2003). Eating disorders. Lancet, 361, 407–416.

Ishikawa, S., Kato, M., Tokuda, T., Momoi, H., Sekijima, Y., Higuchi, M., & Yanagisawa, N. (1999). Licorice-induced hypokalemic myopathy and hypokalemic renal tubular damage in anorexia nervosa. International Journal of Eating Disorders, 26(1), 111–114.

Marcussen, N. (1992). Atubular glomeruli and the structural basis for chronic renal failure. Laboratory Investigation, 66(3), 265–284.

Rennke, H.G. (1988). Glomerular adaptations to renal injury or ablation. Role of capillary hypertension in the pathogenesis of progressive glomerulosclerosis. Blood Purification, 6(4), 230–239.

Riemenschneider, T., & Bohle, A. (1983). Morphologic aspects of low-potassium and low-sodium nephropathy. Clinical Nephrology, 19(6), 271–279.

Sharp, C.W., & Freeman, C.P. (1993). The medical complications of anorexia nervosa. British Journal of Psychiatry, 162, 452–462.

Tsuchiya, K., Nakauchi, M., Hondo, I., & Nihei, H. (1995). Nephropathy associated with electrolyte disorders. Nippon Rinsho, 53(8), 1995–2000.

Case Report

Acta Haematologica

Acta Haematol 2005;113:255–257
DOI: 10.1159/000084679

Received: May 25, 2004
Accepted after revision: October 19, 2004

Fatal Splenic Rupture Caused by Infiltration of Adult T Cell Leukemia Cells

Kosei Arimura[a] Naomichi Arima[b] Toshimasa Kukita[a] Hirosaka Inoue[a]
Akihiko Arai[a] Kakushi Matsushita[a] Shuuhei Taguchi[c] Hiroki Yoshida[c]
Atsuo Ozaki[a] Hideaki Kawada[a] Masaki Akimoto[a] Chuwa Tei[d]

[a]Department of Hematology and Immunology, Kagoshima University Hospital; [b]Division of Host Response, Center for Chronic Viral Diseases; [c]Department of Tumor Pathology, and [d]Department of Cardiovascular, Respiratory and Metabolic Medicine, Graduate School of Medical and Dental Sciences, Kagoshima University, Kagoshima, Japan

Key Words
Splenic rupture · Adult T cell leukemia · Splenomegaly · Infiltration

Abstract
The spleen is an immunological organ commonly involved in both hematological and nonhematological diseases. Pathological rupture of the spleen has been described in a variety of diseases affecting the spleen. Infections have been cited in most cases involving splenic rupture, but are rare in hematological malignancies despite frequent involvement of the spleen. The present report describes a fatal case of splenic rupture caused by infiltration of adult T cell leukemia cells and reports the mechanism of splenic rupture. The importance of rapid diagnosis and surgery is emphasized.

Introduction

Pathological rupture of the spleen has been reported in a large number of diseases [1–4], including infectious mononucleosis [5] and malaria [6]. However, reports of hematological malignancy-induced rupture of the spleen are very rare, despite the frequent involvement of the spleen in such diseases [1–4]. The present report describes a fatal case of splenic rupture caused by infiltration of adult T cell leukemia (ATL) cells.

Case Report

A 53-year-old woman noticed a facial eruption near her nose, and presented to our hospital in 1999. Laboratory examination revealed abnormal lymphocytes comprising 15% of the leukocytes. Serum human T-lymphotropic virus type 1 (HTLV-1) antibody results were positive, while serum lactate dehydrogenase (sLD) levels were within the normal range. Chronic ATL was therefore diagnosed [7]. In June 2002, cervical lymph nodes became swollen and sLD levels were elevated, although the patient displayed no other symptoms. She was admitted to our hospital and treated using combined chemotherapy with biweekly CHOP [8], but treatment was unsatisfactory. In December 2002, ATL cells were increased in peripheral blood, sLD levels were elevated, white blood cell count (WBC) was 63.5 × 10^9/l and sLD level was 9,930 IU/l. After a few days, splenomegaly appeared for the first time since onset, along with sudden and severe anemia, and hemoglobin concentration decreased to 5.0 g/dl. However, no abdominal pain was reported. The patient died from multiple organ failure, and postmortem examination was performed in January 2003.

The spleen weighed 1,236 g, and was greatly enlarged with a 10-cm-long crack apparent along the inferior edge. About 500 ml of bloody ascites was present. Microscopically, diffuse infiltration of ATL cells was observed in the spleen, including the capsule (fig. 1a). The capsule of the spleen was thin due to splenomegaly and partially ruptured (fig. 1b). In another part, ATL cells had pen-

KARGER
Fax +41 61 306 12 34
E-Mail karger@karger.ch
www.karger.com

0001–5792/05/1134–0255$22.00/0

Accessible online at:
www.karger.com/aha

Naomichi Arima, MD, PhD
Division of Host Response, Center for Chronic Viral Diseases
Graduate School of Medical and Dental Sciences, Kagoshima University
Sakuragaoka 8-35-1, Kagoshima, 890-8520 (Japan)
Tel. +81 99 275 5945, Fax +81 99 275 5947, E-Mail nao@m2.kufm.kagoshima-u.ac.jp

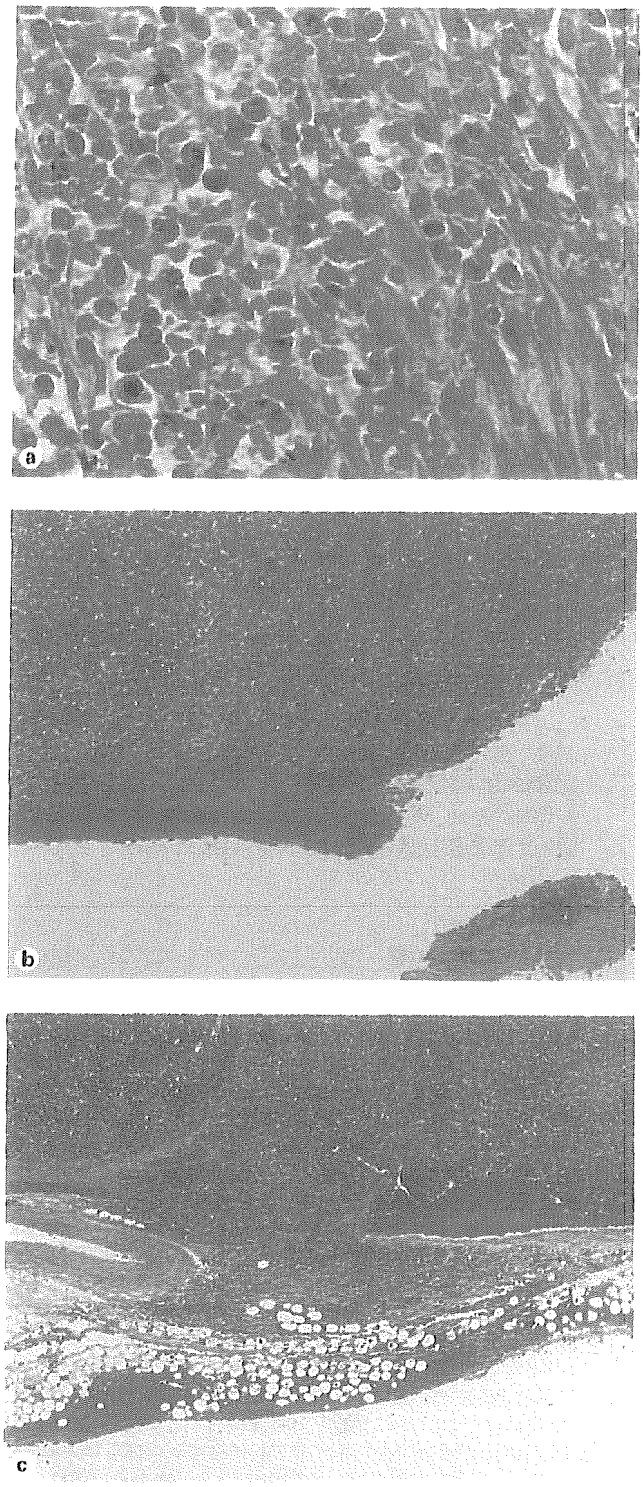

Fig. 1. Pathological findings of spleen. HE. **a** Diffuse infiltration of ATL cells was observed in the spleen, including the capsule. **b** The capsule of the spleen was thin due to splenomegaly and partially ruptured. **c** ATL cells had penetrated the capsule.

etrated the capsule (fig. 1c). Coagulated necrosis and intracapsular bleeding were also apparent. No evidence of infection was identified, including cytomegalovirus, bacteria or fungus. Generalized lymphadenopathy was noted, with pathological infiltration of ATL cells. Infiltration of ATL cells in the heart, lung, liver, kidney, pancreas, uterus, ovary and bone marrow was also found. The stomach and intestines were intact, with no evidence of ATL.

Discussion

The spleen is an immunological organ commonly involved in both hematological and nonhematological diseases. Pathological rupture of the spleen has been associated with a wide variety of underlying conditions, and the phenomenon is uncommon but frequently fatal [9]. While infectious diseases including infectious mononucleosis [5] and malaria [6] have been the most commonly reported disorders associated with splenic rupture, associations with sarcoidosis [10], connective tissue disorders [11, 12] and amyloidosis [13] have also been reported. However, hematological malignancies rarely cause splenic rupture, despite the frequent involvement of the spleen in these diseases [1–4]. This is somewhat surprising, since splenomegaly is a common feature in most hematological diseases, with the spleen sometimes reaching up to 7 kg [3]. Giagounidis et al. [3] reported 136 cases of pathological splenic rupture since 1861, with 34% in acute leukemia, 34% in non-Hodgkin's lymphoma, and 18% in chronic myelogenous leukemia. They also reported higher frequency in males, with a male:female ratio of 3:1, and considerable differences according to specific diseases. Pathological rupture of the spleen has occurred almost exclusively in adults and most ruptured spleens display moderate to severe enlargement [3].

ATL is a hematological malignancy related to HTLV-1 infection. Prognosis in ATL is very poor [7]. The disease is often accompanied by nodal and extranodal lymphomas. In addition, ATL cells often infiltrate into multiple organs, including the spleen [14]. However, reports of pathological rupture of the enlarged spleen in such cases are very rare. Regarding T cell malignancies, only 2 cases of splenic rupture, caused by peripheral T cell lymphoma [2] and mycosis fungoides [15], have previously been reported. To the best of our knowledge, the present report is the first to describe pathological rupture of the spleen due to infiltration of ATL cells.

The precise mechanism of splenic rupture in hematological malignancies is unclear. Recently, Debnath et al. [16] conducted a review that identified 352 cases reported between 1966 and 2000. The spleen is a friable vascu-

lar organ, and has been suggested to be particularly susceptible to parenchymal bleeding when the architecture is damaged by disease, trauma or vascular obstruction and infection, notably in settings of coexistent coagulation disorder. Factors that might explain pathological splenic rupture in hematological malignancies include: (1) infiltration into the spleen of tumor cells changing the histological structure of the spleen; (2) splenic infarction inducing severe structural weakness, and (3) local coagulation disorders leading to intrasplenic and subcapsular bleeding, ultimately resulting in capsular rupture [17]. Coagulation disturbance or thrombocytopenia may play major roles in the pathogenesis of splenic rupture. However, correlations between splenic rupture and coagulation disturbances have not yet been confirmed in any cases. In addition, thrombocytopenia does not seem to increase the risk of splenic rupture. A review by Bauer et al. [17] found no significant correlation between survival and platelet number, leukocyte count, or size of the spleen.

In normal Japanese 50- to 54-year-old females, the mean weight of the spleen is 83.3 ± 34.0 g [18]. The spleen is enclosed within the capsule. In the present case, the spleen weighed 1,236 g at autopsy. Even if the spleen undergoes a considerable increase in size, this internal organ does not rupture easily. Autopsy in the present case revealed ATL cells diffusely infiltrating throughout the spleen and penetrating the capsule. In addition, the capsule of the spleen was stretched and thin due to splenomegaly. However, no splenic infarction or intrasplenic or subcapsular bleeding was identified. These results strongly suggest that thinning of the capsule due to rapid splenomegaly and direct infiltration of ATL cells penetrating the capsule caused splenic rupture in the present case.

Emergency splenectomy represents the only feasible treatment for splenic rupture. Among 136 cases of pathological splenic rupture reported in the literature, 88 patients underwent surgical intervention, while 43 patients were managed without operation. No information could be obtained for the 5 remaining cases. Of the 88 patients who underwent surgical intervention, 55 (63%) survived and 33 (37%) died. Of the 43 patients who did not undergo surgery, 40 died [3]. Splenic surgery in patients with hematological malignancy carries a high mortality and morbidity, due to an increased risk of hemorrhage and infection. In patients with hematological malignancy, pathological rupture of the spleen often happens unexpectedly, with no preceding trauma. Diagnosis is therefore often difficult. The present case displayed a sudden decrease in blood pressure, but no abdominal pain. Careful observation, particularly at the end stage accompanying rapid tumor growth, is therefore necessary when splenic rupture is deemed possible. Using ultrasonography or computer tomography, peritoneal aspiration of fresh blood may assist in the diagnosis of pathological splenic rupture. When the diagnosis is made, emergency splenectomy should be performed.

References

1 Lieberman ME, Levitt A: Spontaneous rupture of the spleen: A case report and literature review. Am J Emerg Med 1989;7:28–31.
2 Schiødt I, Duun E, Fischer TK, Christiansen AP, Ralfkiaer E: Fatal rupture of the spleen caused by infiltration of T-cell lymphoma. Ann Hematol 2000;79:158–160.
3 Giagounidis AAN, Burk M, Meckenstock G, Koch AJ, Schneider W: Pathologic rupture of the spleen in hematologic malignancies: Two additional cases. Ann Hematol 1996;73:297–302.
4 Knoblich R: Pathologic (so-called spontaneous) rupture of spleen in leukaemia and lymphoma. Mich Med 1966;65:105–114.
5 Papesch M, Watkins R: Epstein-Barr virus infectious mononucleosis. Clin Otolaryngol 2001;26:3–8.
6 Zingman BS, Viner BL: Splenic complications in malaria: Case report and review. Clin Infect Dis 1993;16:223–232.
7 Shimoyama M: Diagnostic criteria and classification of clinical subtypes of adult T-cell leukaemia-lymphoma. A report from the Lymphoma Study Group (1984–1987). Br J Haematol 1991;79:428–437.
8 Tobinai K: Chemotherapy: the more, the better in malignant lymphoma? Cancer Chemother Pharmacol 1997;40:110–114.
9 Hyun BH, Varga CF, Rubin RJ: Spontaneous and pathologic rupture of the spleen. Arch Surg 1977;104:652–657.
10 Lam KY, Ng WF, Chan AC: Miliary tuberculosis with splenic rupture: A fatal case with hemophagocytic syndrome and possible association with long standing sarcoidosis. Pathology 1994;26:493–496.
11 Fishman D, Isenberg DA: Splenic involvement in rheumatic diseases. Semin Arthritis Rheum 1997;27:141–155.
12 Karassa FB, Isenberg DA: Spontaneous rupture of the spleen: An unusual complication of systemic lupus erythematosus. Lupus 2001;10:876–878.
13 Oran B, Wright DG, Seldin DC, McAneny D, Skinner M, Sanchorawala V: Spontaneous rupture of the spleen in AL amyloidosis. Am J Hematol 2003;74:131–135.
14 Shimamoto Y, Yamaguchi M: HTLV-I induced extranodal lymphomas. Leuk Lymphoma 1992;7:37–45.
15 Bennett SR, Greer JP, Stein RS, Glick AD, Cousar JB, Collins RD: Death due to splenic rupture in suppressor cell mycosis fungoides: A case report. Am J Clin Pathol 1984;82:104–109.
16 Debnath D, Valerio D: Atraumatic rupture of the spleen in adults. R Coll Surg Edinb 2002;47:437–445.
17 Bauer TW, Haskins GE, Armitage JO: Splenic rupture in patients with hematologic malignancies. Cancer 1981;48:2729–2733.
18 Ogiu N, Nakamura Y, Ijiri I, Hiraiwa K, Ogiu T: A statistical analysis of the internal organ weights of normal Japanese people. Health Phys 1997;72:368–383.

Journal of Neurochemistry, 2005, **92**, 759–766 doi:10.1111/j.1471-4159.2004.02924.x

A gene-targeted mouse model for chorea-acanthocytosis

Yuko Tomemori,* Mio Ichiba,* Akira Kusumoto,* Emiko Mizuno,* Daisuke Sato,* Shinji Muroya,* Masayuki Nakamura,* Hiroaki Kawaguchi,† Hiroki Yoshida,† Shu-ichi Ueno,‡ Kazuki Nakao,§ Kenji Nakamura,¶ Atsu Aiba,** Motoya Katsuki†† and Akira Sano*

*Departments of *Psychiatry and †Pathology, Kagoshima University Graduate School of Medical and Dental Sciences, Kagoshima, Japan*

‡Department of Psychiatry, Course of Integrated Brain Sciences, University of Tokushima School of Medicine, Tokushima, Japan

§Laboratory for Animal Resources and Genetic Engineering, Riken Center for Developmental Biology, Kobe, Japan

¶Reproductive Engineering Section, Mitsubishi Kagaku Institute of Life Sciences, Tokyo, Japan

***Division of Cell Biology, Department of Molecular and Cellular Biology, Kobe University Graduate School of Medicine, Kobe, Japan*

††National Institute for Basic Biology, Okazaki, Japan

Abstract

Chorea-acanthocytosis (CHAC) is a hereditary neurodegenerative disorder with autosomal recessive transmission, in which selective degeneration of striatum has been reported in brain pathology. Clinically, CHAC shows Huntington's disease-like neuropsychiatric symptoms and red blood cell acanthocytosis. Recently, we identified the gene, *CHAC*, encoding a novel protein, chorein, in which a deletion mutation was found in Japanese families with CHAC. In the present study, we have identified the mouse *CHAC* cDNA sequence and the exon–intron structures of the gene and produced a CHAC model mouse introducing no. 60–61 exon deletion corresponding to a human disease mutation by a gene-targeting technique. The mice began to show acanthocytosis and motor disturbance in old age. In behavioral observations, locomotor activity was significantly decreased and the contact time at social interaction test was decreased significantly in the model mice. In the brain pathology, many apoptotic cells were observed in the striatum of the mutant mice. In neurochemical determinations, the dopamine metabolite, homovanillic acid, concentration decreased significantly in the portion including the midbrain of the mutant mice. These findings are consistent with the human results reported elsewhere and indicate that the CHAC model mice showed a mild phenotype with late adult onset. The CHAC model mouse therefore provides a good model system to study the human disease.

Keywords: *CHAC*, chorea-acanthocytosis, chorein, gene-targeted mouse model, neurodegeneration.

J. Neurochem. (2005) **92**, 759–766.

Chorea-acanthocytosis (CHAC; MIM 200150) is a rare autosomal recessive neurodegenerative disorder, relatively more frequent in Japan (Rampoldi *et al.* 2002). Clinically, CHAC is best characterized by the gradual and adult onset of chorea and acanthocytosis in erythrocytes. In addition, other neuropsychiatric deficits, such as oral dyskinesia and dystonia frequently with self-mutilation, personality change, schizophrenia-like symptoms, dementia, myopathy and peripheral neuropathy, often take place (Brin 1993). Dilated cardiomyopathy has been reported in some patients with CHAC (Kageyama *et al.* 2000). The main neuropathological finding of CHAC is the degeneration of striatum (Hardie *et al.* 1991).

Recently, we and others identified the gene *CHAC* that is responsible for CHAC (Rampoldi *et al.* 2001; Ueno *et al.* 2001). The *CHAC* gene exists on human chromosome 9q21 spanning a 250-kb region and consists of 73 exons. Although

Received August 13, 2004; revised manuscript received October 1, 2004; accepted October 3, 2004.

Address correspondence and reprint requests to Akira Sano, MD, PhD, Department of Psychiatry, Kagoshima University Graduate School of Medical and Dental Sciences 8-35-1 Sakuragaoka, Kagoshima 890-8520, Japan. E-mail: sano@m3.kufm.kagoshima-u.ac.jp

Abbreviations used: CHAC, chorea-acanthocytosis; HVA, homovanillic acid; TUNEL, terminal transferase biotinylated-UTP nick end-labeling.

the function of chorein, the product of *CHAC*, is unclear, the homologs have been found in *Saccharomyces cerevisiae* and *Dictyosteium discoideum* (Brickner *et al.* 1997). The null mutant of the *S. cerevisiae* homolog *VPS13* is viable but shows defects in vacuolar protein sorting and a *TipC* gene mutant of *D. discoideum* has aberrant cell-sorting behavior so chorein is thought to play a role in the dynamic change of cellular structures.

Chorea-acanthocytosis is very rare and the number of autopsied cases is limited, so it is difficult to study the molecular pathogenesis of CHAC using human specimens. Therefore, the CHAC model mouse is very valuable. Here we report the production and characterization of a *CHAC* mutant mouse which carries a CHAC-causative Ehime deletion mutation found in Japanese patients with CHAC (Ueno *et al.* 2001).

Materials and methods

Search for mouse homolog of chorea-acanthocytosis gene

To identify the mouse homolog of *CHAC*, we searched the expressed sequence tags (ESTs) on the NCBI database. RT-PCR was carried out with primer setting according to reported mouse EST sequences. Total RNA, for use as RT-PCR template, was extracted from C57BL/6J mouse leukocytes using the QIAamp RNA Blood Mini Kit (Qiagen, Valencia, CA, USA). For detection of the 5′ and 3′ ends, we conducted 5′ RACE (rapid amplification of cDNA ends) and 3′ RACE using the SMART RACE cDNA Amplification Kit (CLONTECH, Palo Alto, CA, USA). Direct sequencing was carried out after RT-PCR.

Generation of the chorea-acanthocytosis deletion mice

We screened a library prepared from 129/Sv mouse genomic DNA (RP22; Invitrogen, Carlsbad, CA, USA) with the use of mouse *CHAC* cDNA. For the construction of the targeting vector of the *CHAC* gene, we subcloned a *PmaCI-SpeI* 8.9-kb genomic DNA fragment. An internal 3.7-kb *ApaI-SalI* fragment including exons 60 and 61, which is deleted in the human CHAC-liable Ehime deletion mutation, was replaced with the neomycin resistance gene. A 1.1-kb diphtheria toxin gene fragment was attached to the 3′ end of the targeting vector for negative selection (Yagi *et al.* 1993). Electroporation of the targeting vector into embryonic stem cells (CCE, 129/Sv background), selection of embryonic stem cells containing the properly targeted gene, generation of 129/Sv/C57BL/6J chimeric mice and germline transmission for the generation of heterozygous mutant F_1 mice in a 129/Sv/C57BL/6J background were carried out as previously described (Koera *et al.* 1997). A typing PCR of the *CHAC* genes was carried out using tail DNA as the template and

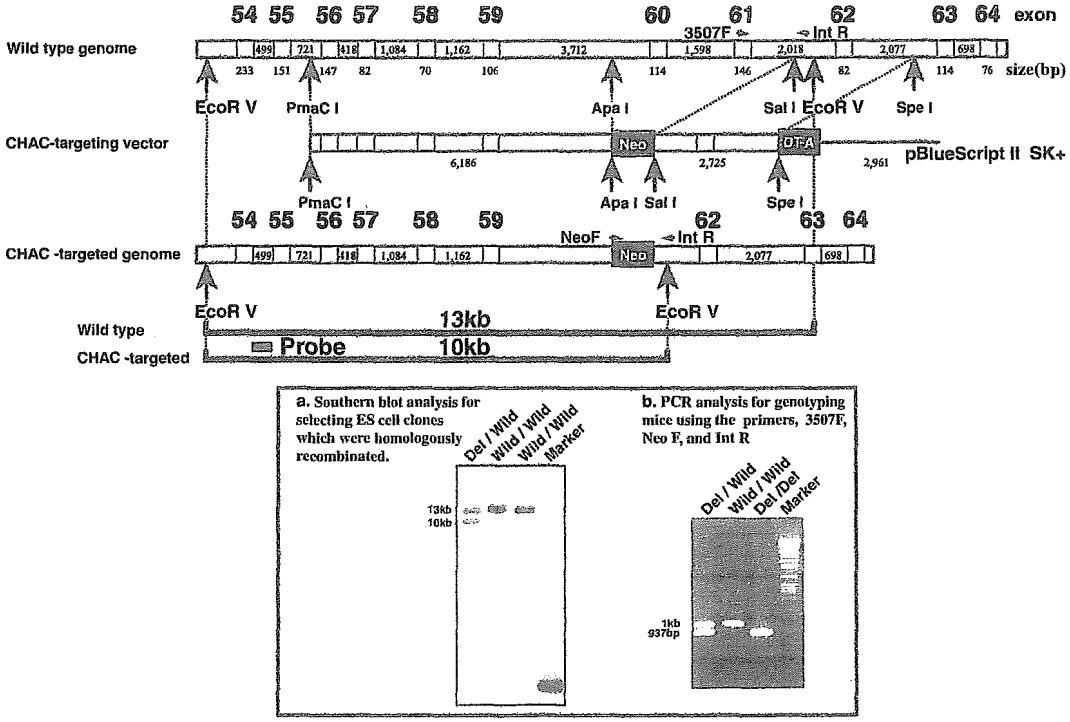

Fig. 1 *Targeted disruption of the CHAC gene. Homologous recombination resulted in replacement of the 3.7-kb fragment including exons 60 and 61 with the neomycin resistance gene (Neo). The diphtheria toxin gene (DT-A) was attached to the 3′ end of the targeting vector for negative selection. Restriction sites are indicated by arrows. The location of the probe used for Southern blot analysis is indicated. EcoRV-digested DNAs were hybridized with the probes. The results of Southern blot analysis for selecting embryonic stem (ES) cell clones and PCR analysis for genotyping mice are shown in the inset.*

primers illustrated in Fig. 1. We observed closely and checked body weight once a week. The use of animals in this research complied with all relevant guidelines of the Japanese government, Institute of Medical Science, University of Tokyo and Kagoshima University.

Osmotic fragility test of red blood cells

Blood was extracted by cutting the axillary vein and collecting in a syringe with heparin to avoid blood coagulation. Each 20 μL was dropped into a gradient concentration of phosphate-buffered NaCl solution (0.85, 0.75, 0.70, 0.65, 0.60, 0.55, 0.50, 0.45, 0.40, 0.35, 0.30, 0.20 and 0.10%, respectively). The hemolytic ratio was calculated by determining the absorbance at 540 nm and the concentration of NaCl (%) to cause 50% hemolysis (C_{50}) was estimated (Try 1980). Results (mean ± SD of seven mutant and nine wild-type mice) are expressed as C50 ± SD.

Footprint pattern

The footprint pattern was used to compare the gait of *CHAC* mutant mice with that of wild-type control mice (Carter *et al.* 1999). To obtain footprints, the hind- and forefeet of the mice were coated with red and green non-toxic paints, respectively. The animals were then allowed to walk along a 50 cm long, 10 cm wide runway (with 10 cm high walls) into an enclosed box. A fresh sheet of white paper was placed on the floor of the runway for each run. Stride length was measured as the average distance of forward movement between each stride. The mean value of each set of three values was used in subsequent analysis ($n = 13$, homozygous mutant mice and $n = 20$, wild-type mice).

Rotarod

The rotarod apparatus (Rotarod; O'Hara & Co., Ltd, Tokyo, Japan) was used to measure fore- and hindlimb motor coordination and balance. Rotarod training consisted of placing the animals on the rotating rod at a speed of 24 r.p.m. for 1 min. Mice received four trials per day for three consecutive days, by which time a steady baseline level of performance was attained (Carter *et al.* 1999). Mice then received two trials at 10 increasing speeds from 15 r.p.m. The mean latency to fall off the rotarod was recorded and used in a subsequent analysis ($n = 13$, homozygous mutant mice and $n = 20$, wild-type mice).

Open field analysis

Animals were put off the rack for 1 h before the test to accustom them to the novel environment and then placed in a box (50 × 50 cm). Traces were drawn for 10 min by an image-analysing program (Image OF4; O'hara & Co., Ltd) and the total moving distance was calculated ($n = 13$, homozygous mutant mice and $n = 20$, wild-type mice).

Social behavior

We conducted a social interaction test between two male mice of the same genotype group. Each group consisted of eight samples. Mice were reared with one to four other mice per cage. After accustoming the mice as described for open field analysis, two mice were placed in a closed 50 × 50 cm box and traces were drawn by the image-analysing programs Image OFC and SI (O'hara & Co., Ltd). The test lasted for 2 min per session and the total moving distances of the mice and contact time were calculated.

Monoamine and amino acid analysis

Brains were removed from *CHAC* mice homozygous for the transgene ($n = 6$) and normal littermate ($n = 6$) controls at 79–84 weeks of age and dissected on ice basically according to the method of Glowinski and Iversen (McIlwain and Voaden 1975). Tissues were stored frozen at − 80°C until analysis for neurotransmitter content. Levels of the monoamine neurotransmitters and metabolites were determined separately by established HPLC methods using electrochemical detection (Reynolds and Pearson 1987). GABA was analysed using the same samples by HPLC coupled to post-column ninhydrin derivatization with spectrophotometry.

Histological analysis

Four homozygous mutant and five wild-type mice (72–84-week-old females) were deeply anesthetized with sodium pentobarbital and perfused through the left ventricle with cold 4% paraformaldehyde in 0.1 M sodium phosphate buffer at pH 7.4. Brain and other organs were removed and post-fixed in the respective perfusion solution overnight at 4°C. The tissues were dehydrated and embedded in paraffin. For imnunohistochemistry coronal sections of the brain were cut on a microtome at 4 μm. Tissue sections were deparaffinized and rehydrated after cutting samples. All brain sections were incubated with methanol containing 0.3% H_2O_2 to block endogenous peroxidase activity and then incubated with a primary antiserum diluted with 0.05 M Tris-buffered saline containing 0.2% Triton X-100 for glial fibrillary acidic protein (1/500; rabbit polyclonal; Dako, Glostrup, Denmark) overnight at 4°C. Immunoreactive products were detected using a Vectastatin ABC Kit (Vector Laboratories, Burlingame, CA, USA) and then visualized after adding DAB (3,3′-Diamino-benzidine tetrohydrochloride) as the chromogen. For Terminal transferase biotinylated-UTP nick end-labeling (TUNEL) stain, we used the Fast Red Substrate System (Dako). Tissue sections were counterstained with hematoxylin. TUNEL-positive cells were counted in five fields on one side of the striatum in six mice (three wild-type and three mutant mice). The number of positive cells was examined by statistical analysis.

Statistical analysis

All statistical analyses were performed using Mann–Whitney's *U*-test for comparisons between wild-type and *CHAC* mutant. All data are presented as mean ± SD.

Results

Cloning of mouse chorea-acanthocytosis homolog

To obtain the mouse homolog of the human *CHAC* gene, various combinations of primers generated from the sequence of the human *CHAC* gene (Ueno *et al.* 2001) were tested using RT-PCR. Some primer sets gave rise to suitable products using cDNA from mouse brain as template. We extended the assembled sequence to both 5′ and 3′ directions by the RACE method. The total number of sequenced nucleotides was 9861 bp (Accession no. DDBJ AB115421).

The ATG at nucleotide residues 160–162 is likely to be the translation initiation codon and an in-frame TGA stop codon is present at nucleotide residues 9658–9660, which suggests that it codes for a protein of 3166 amino acids. The cDNA sequence was compared with the reported mouse genomic sequence (Accession no. NT_039687) and 72 exons with proper consensus exon–intron boundary sequences were confirmed in the genomic sequence.

Gene targeting of chorea-acanthocytosis

In order to produce a CHAC model mouse by introducing the no. 60–61 exon deletion corresponding to a human disease mutation (Ueno *et al.* 2001), we first isolated an 8.9-kb fragment containing mouse *CHAC* exons 60 and 61 from the 129/Sv genomic BAC library. We assembled a targeting vector to replace from the middle of intron 59 to the middle of intron 61 by a neomycin resistance cassette (Fig. 1). The successful deletion was confirmed at genome level by Southern blot (Fig. 1 inset). The consequence of such aberrant splicing in this putative coding mRNA is the change of the open reading frame (ORF) from position codon 2730 and the appearance of a stop codon at position 2735. Germline transmission was obtained with chimeric mice. F_1 and F_2 mice were confirmed by PCR (Fig. 1 inset). Mice carrying the homozygous mutation were viable. We obtained 101 offspring by *CHAC* deletion F_1 heterozygote matings. The genotypes were 20.8% (21/101) homozygous mutant, 35.6% (36/101) wild-type and 43.6% (44/101) heterozygous mutant. There was no segregation distortion between genotypes and no significant difference in survival ratio (Fig. 2) and body weight at the age of 87 weeks. Involuntary movements were not found. Mice with the genotype del/del were used as *CHAC* mutant mice for the experiments below together with wild-type controls.

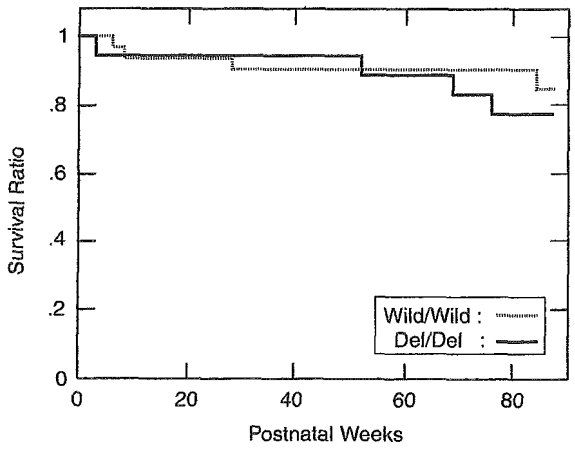

Fig. 2 Survival curve. We obtained 101 F_2 mice consisting of 21 homozygous mutant, 44 heterozygous mutant and 36 wild-type mice. There was no significant difference in survival ratio between wild-type and homozygous mutant mice at the end of observation.

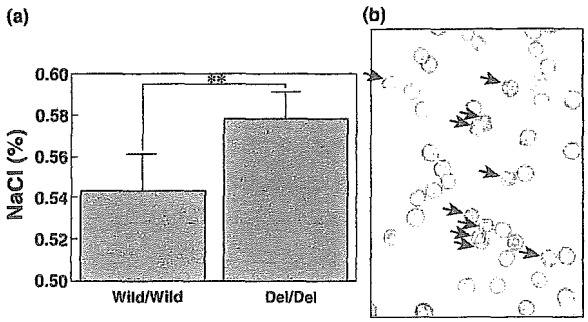

Fig. 3 (a) Osmotic fragility test of red blood cells. Each 20 μL of blood from wild-type and homozygous *CHAC* mutant mice was mixed with 2 mL of phosphate-buffered NaCl solutions with concentrations of 0.85, 0.75, 0.70, 0.65, 0.60, 0.55, 0.50, 0.45, 0.40, 0.35, 0.30, 0.20 and 0.10%, respectively. The hemolytic ratio was calculated by determining the absorbance at 540 nm and the concentration of NaCl (%) to cause 50% hemolysis (C50) was estimated. Results (mean ± SD of 13 mutant and 20 wild-type mice) are expressed as C50 ± SD. Significant difference between wild-type control and *CHAC* mutant mice (**$p < 0.01$). (b) Many acanthocytes indicated by arrows were observed in peripheral blood smears of *CHAC* mutant mice.

Hematological analysis

Light microscopy of red blood cells

Light microscopic observation of peripheral blood smears of *CHAC* mutant mice showed heterogeneity in sizes and shapes of the erythrocytes, including acanthocytes (Fig. 3b).

Osmotic fragility analysis of red blood cells

The osmotic fragility test is the most sensitive test available to detect cells that are less tolerant to osmotic stress than normal cells (Becker and Lux 1995). The red blood cells from *CHAC* mutant mice showed an increase in their *in vitro* osmotic fragility when exposed to hypotonic NaCl solutions. We found that the NaCl concentration that produced 50% hemolysis (C50) was significantly higher in the mutant mice (Fig. 3b). C50 values were 0.578% (w/v) NaCl for *CHAC* mutant mice and 0.543% NaCl for wild-type mice. A marked increase in the osmotic fragility of red blood cells in the *CHAC* mutant mice together with acanthocytosis defines a full set of hematological abnormal findings seen in human CHAC (Palek 1991).

Motor function

Footprint test

Gait disturbance was assessed by analysing the footprint patterns while mice walked along a narrow corridor. Footprint patterns of wild-type and *CHAC* mutant mice at 84–87 weeks of age were illustrated. Wild-type mice walked in a straight line with a regular even alternating gait, placing the hindpaw precisely at the position where the ipsilateral

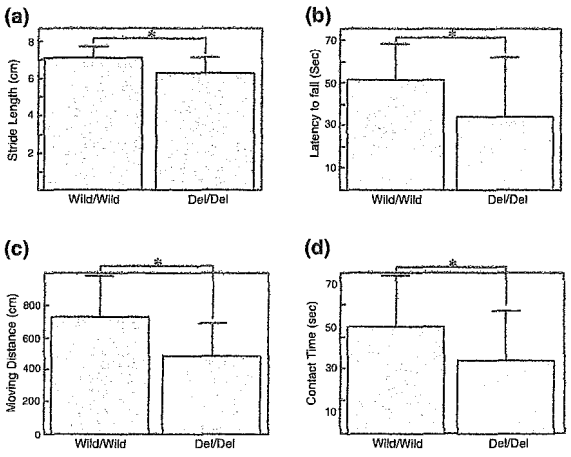

Fig. 4 (a) Quantitative analysis of stride length. Walking footprint patterns were produced by wild-type and *CHAC* mutant mice and stride lengths were then determined. The average stride length of the *CHAC* mutant mice was significantly less than that of wild-type mice (*$p < 0.05$). (b) Balance and motor coordination on the rotarod. Wild-type ($n = 20$) and *CHAC* mutant ($n = 13$) mice were subjected to an accelerating rotarod. The means ± SD of the latency to fall (maximum trial duration, 60 s) for each two trials were recorded. The *CHAC* mutant mice exhibited poorer performance on rotarod than wild-type mice. Significant difference between wild-type control and *CHAC* mutant mice (*$p < 0.05$). (c) Open field analysis. Basal motor activity in control wild-type and *CHAC* mutant mice at 70–82 weeks of age. Locomotor activity measured by moving distance was decreased in the *CHAC* mutant mice (*$p < 0.05$). (d) Social interaction analysis. Each two mice were placed in a closed 50 × 50 cm box and traces drawn by image-analysing programs. The tests lasted for 2 min per session. Total moving distances of the mice and contact time were calculated. Total contact time was significantly decreased in the *CHAC* mutant mice (*$p < 0.05$).

forepaw had been in the previous step. By contrast, *CHAC* mutant mice walked with short steps and their hindpaws were not on the forepaws. The resulting footprint patterns were assessed quantitatively by measuring the stride length. The mean stride length of *CHAC* mutant mice was significantly shorter compared with that of control mice (Fig. 4a, $p < 0.05$).

Rotarod test

Motor coordination and balance of the mice were measured using a rotarod. The mean latency to fall off was significantly shorter in *CHAC* mutant compared with wild-type mice (Fig. 4b, $p < 0.05$). The broad range of SDs showed the existence of differences between individuals.

Locomotor activity and social interaction

Spontaneous locomotor activities in the open field were measured for 10 min in daytime with a behavioral tracing analyser (O'hara & Co., Ltd). The total moving distance in a

Table 1 Monoamines, their metabolites and GABA concentration in brain regions

	Cerebral cortex		Striatum		Hippocampus		Thalamus, hypothalamus midbrain		Cerebellum		Lower brainstem	
	Wild/wild	Del/del	Wild/wild	Del/del	Wild/wild	Del/del	Wild/wild	Del/del	Wild/wild	Del/del	Wild/wild	Del/del
Norepinephrine	215 ± 44	256 ± 26	86 ± 17	89 ± 7	336 ± 36	352 ± 63	461 ± 126	434 ± 60	182 ± 23	200 ± 50	451 ± 68	483 ± 90
Dopamine	402 ± 83	339 ± 144	10 864 ± 1975	9943 ± 1144	14 ± 4	13 ± 2	454 ± 113	350 ± 114	5 ± 1	5 ± 2	27 ± 7	27 ± 5
HVA	149 ± 11	158 ± 22	1082 ± 146	1095 ± 87	48 ± 8	52 ± 7	193 ± 22	160 ± 22*	48 ± 8	40 ± 18	44 ± 7	57 ± 20
5-HT	454 ± 87	384 ± 72	524 ± 145	413 ± 63	536 ± 69	465 ± 35	620 ± 170	611 ± 119	69 ± 33	65 ± 29	410 ± 113	393 ± 126
5-HIAA	325 ± 41	291 ± 12	394 ± 110	366 ± 44	441 ± 67	439 ± 74	763 ± 176	666 ± 61	151 ± 32	138 ± 36	540 ± 82	529 ± 57
GABA	ND	ND	1323 ± 174	1341 ± 316	ND	ND	2605 ± 525	2323 ± 240	ND	ND	ND	ND

Data are mean ± SD values, in ng/g of tissue, from six animals per group. 5-HIAA, 5-hydroxyindoleacetic acid; 5-HT, 5-hydroxytryptamine; HVA, homovanillic acid.
*$p < 0.05$ vs. Wild/Wild.

novel environment in wild-type ($n = 20$) and *CHAC* mutant mice ($n = 13$) showed a significant difference (Fig. 4c, $p < 0.05$). Wild-type mice showed a tendency to spend more time in the center area (data not shown).

In the social interaction test, *CHAC* mutant mice showed less contact time (Fig. 4d, $p < 0.05$) and stayed in the edge area of the field for a significantly longer time.

Atrophy and neurotransmitter analysis in the brain

The weight ratio of one portion : whole brain was measured and we found a significant difference in the striatum. The ratio in *CHAC* mutant mice brain was smaller than that in wild-type mice ($p < 0.05$). Monoamines, their metabolites and GABA were measured from the homogenate of brain sections divided into six portions, hippocampus, striatum, cerebral cortex, cerebellar, brainstem and others (midbrain, thalamus and hypothalamus). Mean values of the dopamine level were less in *CHAC* mutant compared with wild-type mice in both striatum and the portion including midbrain but were not significant (9943 ± 1.144 vs. 10 864 ± 1975 ng/g, $p = 0.346$; 350 ± 114 vs. 454 ± 113 ng/g, $p = 0.142$, respectively). However, the level of the dopamine metabolite homovanillic acid (HVA) in the portion including midbrain was significantly less in the mutant mice (Table 1, $p < 0.05$). Such a mild and insignificant decrease was observed in the level of GABA in the portion including midbrain (2323 ± 240 vs. 2605 ± 525 ng/g; $p = 0.262$).

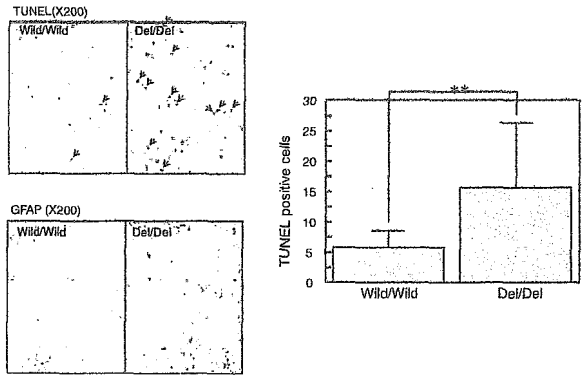

Fig. 5 Terminal transferase biotinylated-UTP nick end-labeling (TUNEL) stain of the striatum of 72–84-week-old wild-type and *CHAC* mutant mice. TUNEL stain, staining the apoptotic cells; many more TUNEL-positive cells were detected in *CHAC* mutant compared with wild-type striatum. Gliosis was found as a marked increase of glial fibrillary acidic protein (GFAP)-immunopositive cells. In TUNEL stain, TUNEL-positive cells in the striatum were counted in every five fields (200 ×) of three wild-type and three *CHAC* mutant mice. The means ± SD of TUNEL-positive cells are shown. There was a significant difference (**$p < 0.001$).

Histopathological and immunohistochemical study of the brain and muscle

In the striatum, remarkable gliosis was detected by anti-glial fibrillary acidic protein antibody in some mutant mice. Apoptosis to a marked degree was detected in the striatum of the mutant mice by the TUNEL staining method. The numbers of TUNEL-positive cells in the striatum of mutant mice were significantly greater than those of wild-type mice (Fig. 5). In some mutant mice, gliosis was marked in the pars reticulata of the substantia nigra (data not shown). These findings were quite similar to the findings in the brain of human CHAC autopsied cases (Hardie *et al.* 1991; Rinne *et al.* 1994).

Discussion

We identified the mouse *CHAC* cDNA sequence and confirmed that the exon–intron organization of the mouse *CHAC* gene is exactly the same as that of the human gene. We then generated and characterized a targeted CHAC model mouse in which exons 60 and 61 of the *CHAC* gene are deleted. The above deletion including exons 60 and 61, Ehime deletion mutation, is found in human Japanese patients suffering from CHAC (Ueno *et al.* 2001). The deletion is present in the coding region of the cDNA resulting in a frame shift and the production of a truncated protein. The *CHAC* mutant mice are viable and reproduce successfully but, after becoming old, they display disturbances in motor function and blood morphological changes which are similar to the features of adult onset and gradual progress seen in human CHAC (Rampoldi *et al.* 2002).

In the present study, the ratio of striatum : whole brain was significantly smaller in the mutant than wild-type mice, which means the selective atrophy of the striatum. Immunohistochemical study of targeted CHAC model mice showed significantly more apoptotic cells in the striatum. The number of TUNEL-positive cells in the striatum of mutant mice was much greater than that of glial fibrillary acidic protein-positive astroglial cells (Fig. 5), which means that most of the TUNEL-positive cells should be neurons. However, intact neuronal cells still seemed to be much more numerous than TUNEL-positive apoptotic cells in mutant mice striatum (Fig. 5), which may explain the discrepancy of normal striatal GABA level in mutant mice (Table 1) despite a marked increase in TUNEL-positive cells. Biochemical analysis showed a significant decrease in HVA concentration in the portion including midbrain of the mutant mice. The main neuropathological finding of CHAC is the degeneration of striatum (Hardie *et al.* 1991). Detailed neuropathological and biochemical findings of human CHAC have only been reported in several autopsy cases. de Yebenes *et al.* (1988) studied neurochemical findings in two autopsy cases of recessive-type neuroacanthocytosis. They determined the levels of monoamines and their metabolites, GABA and

substance P in brain areas. They found depletion of dopamine and its metabolite HVA in the striatum and a marked reduction of HVA in the substantia nigra. Rinne *et al.* (1994) reported the degeneration of the substantia nigra as well as the striatum in some cases of CHAC. The pathological findings in the mutant mouse in the present study coincide well with those in human CHAC mentioned above.

The symptoms and clinical findings of CHAC resemble those of Huntington's disease (Rampoldi *et al.* 2002). Various kinds of model Huntington's disease mice have been produced. Reynolds *et al.* (1999) examined several brain regions of R6/2 transgenic mice, which carry human huntingtin exon 1 including the expanded polyglutamine tract, measuring GABA, glutamate and monoamine neurotransmitters by HPLC. They found that 5-hydroxytryptamine in all brain areas and dopamine in the striatum of older mice decreased, which is related to basal ganglia dysfunction linked to involuntary movements. In this study, *CHAC* mutant mice showed a significant decrease of HVA in the portion including midbrain, thalamus and hypothalamus. Dopamine also decreased but was not significant. Immunohistochemical findings revealed gliosis in the striatum and substantia nigra where degeneration is also found in Huntington's disease (Reddy *et al.* 1998; Lin *et al.* 2001). These results indicate that the dopamine system innervating basal ganglia in *CHAC* mutant mice was impaired. *CHAC* mutant mice did not show any weight loss and showed longevity. However, the results of behavioral analysis indicated the existence of motor dysfunction in old age although the characteristics of motor dysfunction in the mutant mice were distinct from human symptoms seen in CHAC despite the coincidence of the neuropathology. Human patients with CHAC present chorea as the major motor symptom but the model mice showed gait disturbance and early fall from the rotarod without any involuntary movements. Similar discrepancies have been reported repeatedly in many kinds of Huntington's disease model transgenic or knock-in mice (Menalled *et al.* 2002). Phylogenetical differences in the development of basal ganglia may be one of the reasons for the discrepancies in motor function.

Almost complete reproduction of the above human neuropathology in the *CHAC* mutant mouse, together with the phenotypes of motor disturbances and hematological abnormalities, make the model mouse ideal for understanding the molecular pathogenesis of CHAC.

Acknowledgements

The authors thank Ms Tanabe and Mr Kodama for their technical assistance and Dr Izumo for valuable discussion. This work was supported in part by a Grant-in-Aid for Research from the Ministry of Education, Culture, Sports, Science and Technology, Japan.

References

Becker P. S. and Lux S. E. (1995) Hereditary spherocytosis and hereditary elliptocytosis, in *The Metabolic Basis of Inherited Disease* (Scriver C. R. and Beaudet A. L., eds), pp. 3513–3560. McGraw-Hill, New York.

Brickner J. H. and Fuller R. S. (1997) SOI1 encodes a novel conserved protein that promotes TGN-endosomal cycling of Kex2p and other membrane proteins by modulating the function of two TGN localization signals. *J. Cell Biol.* **139**, 23–36.

Brin M. F. (1993) Acanthocytosis, in *Handbook of Clinical Neurology* (Goetz C. G., Tanner C. M. and Aminoff M. J., eds), Vol. 63, pp. 271–299. Elsevier Science B.V., Amsterdam.

Carter R. J., Lione L. A., Humby T. *et al.* (1999) Characterization of progressive motor deficits in mice transgenic for the human Huntington's disease mutation. *J. Neurosci.* **19**, 3248–3257.

Hardie R. J., Pullon H. W., Harding A. E. *et al.* (1991) Neuroacanthocytosis. A clinical, haematological and pathological study of 19 cases. *Brain* **114**, 13–49.

Kageyama Y., Kodama Y., Tadano M., Yamamoto S. and Ichikawa K. (2000) A case of chorea-acanthocytosis with dilated cardiomyopathy and myopathy. *Rinsho Shinkeigaku* **40**, 816–820.

Koera K., Nakamura K., Nakao K., Miyoshi J., Toyoshima K., Hatta T., Otani H., Aiba A. and Katsuki M. (1997) K-Ras is essential for the development of the mouse embryo. *Oncogene* **15**, 1151–1159.

Lin C. H., Tallaksen-Greene S., Chien W. M., Cearley J. A., Jackson W. S., Crouse A. B., Ren S., Li X. J., Albin R. L. and Detloff P. J. (2001) Neurological abnormalities in a knock-in mouse model of Huntington's disease. *Hum. Mol. Genet.* **10**, 137–144.

McIlwain H. and Voaden M. J. (1975) Dissection of the brain to regional blocks, in *Practical Neurochemistry* (McIlwain H., ed.), pp. 284–289. Churchill Livingstone, New York.

Menalled L. B., Sison J. D., Wu Y. *et al.* (2002) Early Motor dysfunction and striosomal distribution of huntingtin Micro aggregates in Huntington's disease Knock-in Mice. *J. Neursci.* **22**, 8266–8276.

Palek J. (1991) Red cell membrane disorders, in *Hematology: Basic Principles and Practice* (Hoffman R., Benz E. J. Jr, Furie B., Shattil S., Cohen H., eds), pp. 472–504. Churchill Livingstone, New York.

Rampoldi L., Dobson-Stone C., Rubio J. P. *et al.* (2001) A conserved sorting-associated protein is mutant in chorea-acanthocytosis. *Nat. Genet.* **28**, 119–120.

Rampoldi L., Danek A. and Monaco A. P. (2002) Clinical features and molecular bases of neuroacanthocytosis. *J. Mol. Med.* **80**, 475–491.

Reddy P. H., Williams M., Charles V., Garrett L., Pike-Buchanan L., Whetsell W. O. Jr, Miller G. and Tagle D. A. (1998) Behavioural abnormalities and selective neuronal loss in HD transgenic mice expressing mutated full-length HD cDNA. *Nat. Genet.* **20**, 198–202.

Reynolds G. P. and Pearson S. J. (1987) Decreased glutamic acid and increased 5-hydroxytryptamine in Huntington's disease brain. *Neurosci. Lett.* **78**, 233–238.

Reynolds G. P., Dalton C. F., Tillery C. L., Mangiarini L., Davies S. W. and Bates G. P. (1999) Brain neurotransmitter deficits in mice transgenic for the Huntington's disease mutation. *J. Neurochem.* **72**, 1773–1776.

Rinne J. O., Daniel S. E., Scaravilli F., Harding A. E. and Marsden C. D. (1994) Nigral degeneration in neuroacanthocytosis. *Neurology* **44**, 1629–1632.

Try K. (1980) Lineation of the osmotic fragility curve of erythrocytes. *Scand. J. Haematol.* **24**, 157–161.

Ueno S., Maruki Y., Nakamura M., Tomemori Y., Kamae K., Tanabe H., Yamashita Y., Matsuda S., Kaneko S. and Sano A. (2001) The gene

encoding a newly discovered protein, chorein, is mutated in chorea-acanthocytosis. *Nat. Genet.* **28**, 121–122.

Yagi T., Nada S., Watanabe N., Tamemoto H., Kohmura N., Ikawa Y. and Aizawa S. (1993) A novel negative selection for homologous recombinants using diphtheria toxin A fragment gene. *Anal. Biochem.* **214**, 77–86.

de Yebenes J. G., Brin M. F., Mena M. A. *et al.* (1988) Neurochemical findings in neuroacanthocytosis. *Mov. Disord.* **3**, 300–312.

American Journal of Pathology, Vol. 168, No. 3, March 2006

DOI: 10.2353/ajpath.2006.050801

Matrix Pathobiology

Discoidin Domain Receptor 1 Contributes to the Survival of Lung Fibroblast in Idiopathic Pulmonary Fibrosis

Wataru Matsuyama, Masaki Watanabe, Yuko Shirahama, Hideo Mitsuyama, Ikkou Higashimoto, Mitsuhiro Osame, and Kimiyoshi Arimura

From the Division of Respiratory Medicine, Respiratory and Stress Care Center, Kagoshima University Hospital, Kagoshima, Japan

Idiopathic pulmonary fibrosis (IPF), characterized by fibroblast proliferation and accumulation of extracellular matrix, including collagen, is a chronic progressive disorder that results in lung remodeling and fibrosis. However, the cellular mechanisms that may make fibroblasts resistant to apoptosis have not been completely elucidated. Discoidin domain receptor 1 (DDR1), a receptor tyrosine kinase whose ligand is collagen, is expressed *in vivo* and contributes *in vitro* to leukocyte differentiation and nuclear factor (NF)-κB activation, which may play an important role in fibroblast survival. In this study, we examined *in vivo* and *in vitro* DDR1 expression and its role in cell survival using fibroblasts obtained from IPF and non-IPF patients. Immunohistochemically, fibroblasts present in fibroblastic foci expressed endogenous DDR1. The DDR1 expression level was significantly higher in fibroblasts from IPF patients, and the predominant isoform was DDR1b. In IPF patients, DDR1 activation in fibroblasts inhibited Fas ligand-induced apoptosis and resulted in NF-κB nuclear translocation. Suppression of DDR1 expression in fibroblasts by siRNA abolished these effects, and an NF-κB inhibitor abrogated the anti-apoptotic effect of DDR1 activation. We propose that DDR1 contributes to fibroblast survival in the tissue microenvironment of IPF and that DDR1 up-regulation may occur in other fibroproliferative lung diseases as well. *(Am J Pathol 2006, 168:866–877; DOI: 10.2353/ajpath.2006.050801)*

Idiopathic pulmonary fibrosis (IPF) is a progressive and usually fatal pulmonary disorder that is characterized by fibroblast proliferation and abnormal accumulation of extracellular matrix (ECM) molecules, particularly fibrillar collagens.[1] An important feature of IPF is the presence of fibroblast foci, which are widely distributed throughout the lung parenchyma.[1] The fibroblastic foci represent microscopic zones of acute lung injury (ALI) in which fibroblasts migrate, proliferate, and contribute to the accumulation of ECM molecules in the damaged alveolus. Subsequently, abnormal remodeling of the lung architecture results from interstitial and intraluminal deposition of connective tissue.[2] In these processes, the release of fibrogenic cytokines may result in fibroblast proliferation and migration to various sites in the lung, followed by differentiation of the fibroblast phenotype.[3,4] This differentiation of fibroblasts is considered key to the chronic nature of IPF, and several reports suggest that fibroblasts in IPF appear to be more resistant to apoptosis,[5,6] a process that is important in both the pathogenesis and resolution of pulmonary fibrotic lesions.[7] However, the cellular mechanisms specifically involved in fibroblast apoptosis have not been completely elucidated. Furthermore, the assumption that fibroblasts in IPF are more resistant to apoptosis remains controversial to date.

Discoidin domain receptor 1 (DDR1) is a receptor tyrosine kinase that is activated by binding with its ligand, collagen.[8,9] DDR1 has a unique extracellular domain that is homologous to discoidin 1 of *Dictyostelium discoideum*.[10] DDR1 is constitutively expressed in normal tissues such as lungs, kidneys, colon, and brain; in tumor cells of epithelial origins, such as those from mammary, ovarian, and lung carcinomas[10]; and also in dermal fibroblasts.[11] Five DDR1 isoforms (a, b, c, d, and e) can be generated by alternative splicing of the *DDR1* gene,[10,12] and two of these isoforms (1a and 1b) have known func-

Supported by the Japan Society for the Promotion of Science (grant-in-aid for scientific research no. 16790447), The Sumitomo Foundation (grant no. 040010), the Nagao Memorial Fund, the Uehara Memorial Foundation, and the Kanae Foundation for Life and Socio-Medical Science.

Accepted for publication October 28, 2005.

Address reprint requests to Wataru Matsuyama, Division of Respiratory Medicine, Respiratory and Stress Care Center, Kagoshima University Hospital, Sakuragaoka 8-35-1, Kagoshima 890-8520, Japan. E-mail: vega@xa2.so-net.ne.jp.

tions.[13,14] The DDR1a and DDR1b isoforms differ from each other by an in-frame insertion of 111 bp that codes for an additional 37-amino acid peptide in the proline-rich juxtamembrane region. The 37-amino acid insertion in DDR1b contains the LXNPXY motif that corresponds to the consensus-binding motif of the Shc phosphotyrosine-binding domain.[10] Disruption of the *DDR1* gene in mice resulted in viable animals that were significantly smaller in size than their littermates, whereas female DDR1-null mice showed defects in blastocyst implantation and mammary gland development.[15] These previous observations indicate that DDR1 contributes to tissue development. In addition, we recently found that DDR1b activation can induce leukocyte differentiation[16] and activate transcriptional factor nuclear factor (NF)-κB,[17] which is reported to play an important role in fibroblast survival.[18]

In this study, we obtained primary cultures of fibroblasts from IPF patients and non-IPF patients and examined the DDR1 expression. We observed that fibroblasts obtained from IPF patients predominantly expressed DDR1b and DDR1 activation on IPF fibroblasts inhibited Fas ligand (FasL)-induced apoptosis.

Materials and Methods

This study was reviewed and approved by the Kagoshima University Faculty of Medicine Committee on Human Research.

Immunohistochemistry

Biopsied lung tissues obtained from three IPF patients and three non-IPF patients were examined for the presence of DDR1 by immunohistochemical staining using rabbit anti-DDR1 antibodies (Santa Cruz Biotechnology, Santa Cruz, CA) and visualized by the diaminobenzidine method, as described previously.[19] Briefly, 4-μm-thick sections were mounted on poly-L-lysine-coated slides, dewaxed, and washed in Tris-buffered saline (pH 7.4) for 10 minutes. For optimal antigen retrieval, the sections were pressure cooked in 0.01 mol/L citrate buffer (pH 6.0) for 90 seconds. Endogenous peroxidase activity was blocked using a 3% hydrogen peroxide solution in methanol for 10 minutes. After two washes in phosphate-buffered saline (PBS) containing 1% saponin, the blocking reaction was performed as reported previously.[20] The sections were incubated with a 1:50 dilution of the primary antibody solution for 2 hours at room temperature. Negative control slides were incubated with rabbit IgG (R&D Systems, Minneapolis, MN). Secondary biotinylated anti-immunoglobulin antibodies (R&D Systems) were added, and the mixture was incubated for 30 minutes at room temperature. After washing, the sections were incubated with streptavidin conjugated to horseradish peroxidase (Amersham, Arlington Heights, IL) and then rinsed with deionized water. Diaminobenzidine substrate solution was added, and the mixture was incubated for 10 minutes. A positive result was indicated by a brown color reaction.

Patients with Lung Fibrosis

Fibroblasts were derived from lung tissue samples obtained from seven IPF patients. The lung tissue samples were obtained by video-assisted lung biopsy for diagnosis. IPF was diagnosed in accordance with the American Thoracic Society/European Respiratory Society consensus criteria,[21,22] including the characteristic morphology of usual interstitial pneumonia. The average age of the seven patients (six men and one woman) was 59.5 years (range, 47 to 68 years). Of the seven patients, six were ex-smokers and one was a nonsmoker. None of the patients were treated with immunosuppressive drugs, including corticosteroids.

Non-IPF Patients

Fibroblasts were derived from lung tissue samples obtained from six patients (four men and two women) undergoing lung surgery for the removal of a primary lung tumor. Normal lung tissue from a noninvolved segment, at a distance from the solitary lesion, was obtained. The average age of the six patients was 62.4 years (range, 41 to 70 years); two patients were nonsmokers and four were ex-smokers.

Acute Lung Injury (ALI) Patients

Fibroblasts were also derived from lung samples obtained from four patients who suffered from adult respiratory distress syndrome (two biopsy samples and two autopsy samples). The average age of the four patients was 52.3 years (range, 31 to 61 years). All of the patients were nonsmokers.

Culture of Fibroblasts

Human lung fibroblasts were cultured from lung explants according to the method described by Akamine and colleagues.[23] The fibroblasts were cultured in Dulbecco's modified Eagle's medium containing 10% fetal calf serum supplemented with 100 U/ml penicillin and 100 g/ml streptomycin (complete medium). The cells were used at passage 5. All of the cell cultures were immunohistochemically evaluated at passage 5. Essentially, 100% of the cells were fibroblasts as indicated by the strong labeling with anti-prolyl-4-hydroxylase, anti-vimentin, and anti-CD90 monoclonal antibodies (PharMingen, San Diego, CA).[24] Staining with anti-smooth muscle myosin heavy chain-1, anti-cytokeratin, and anti-CD31 antibodies (PharMingen) was always negative, indicating that the cultures did not contain smooth muscle cells or epithelial or endothelial cells.

Flow Cytometry Analysis

To detect DDR1 and α-smooth muscle actin (α-SMA) expression on fibroblasts, 5×10^5 cells were collected after five passages. The cells were washed three times with PBS and then incubated with human serum (pooled

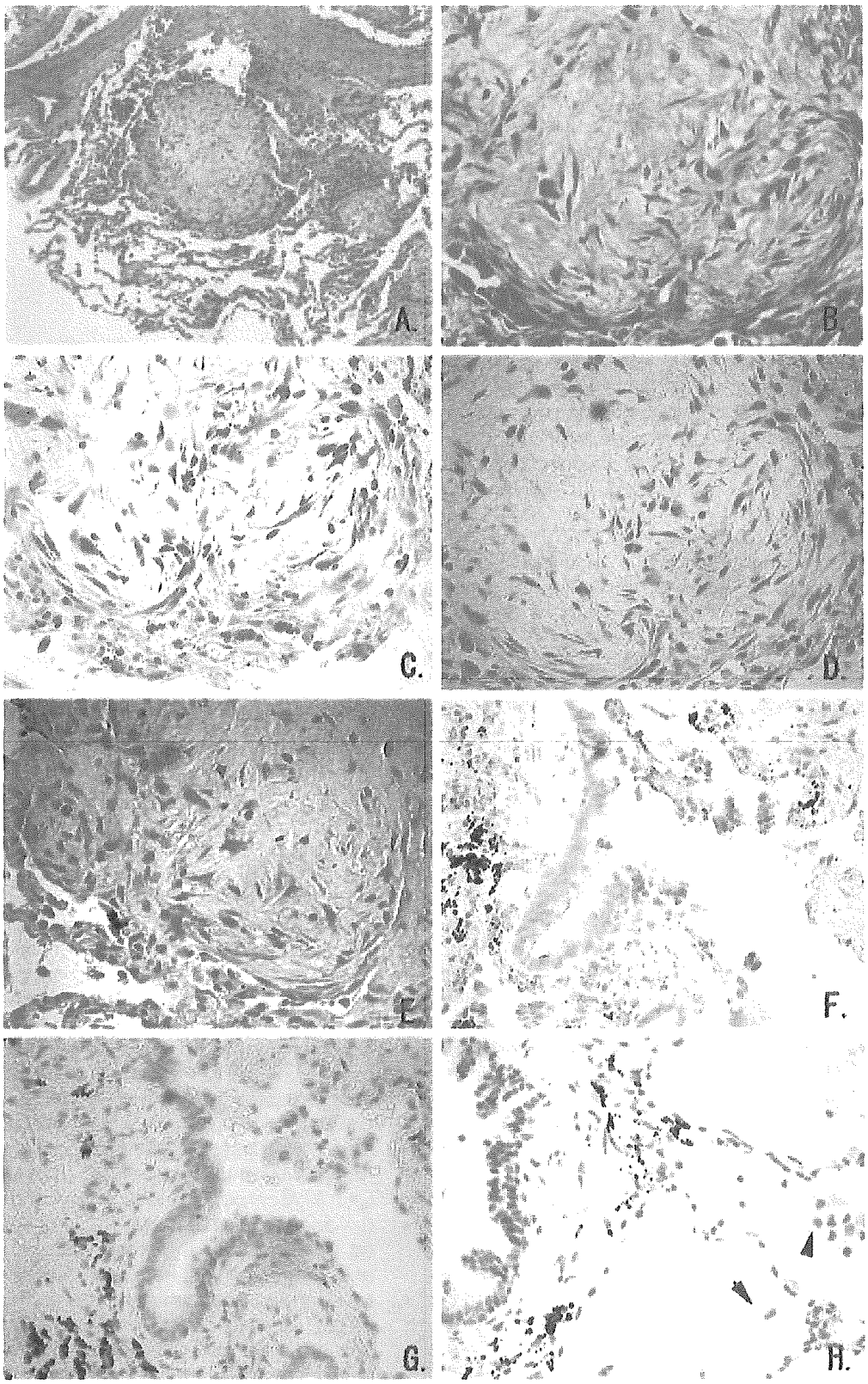

Figure 1. Immunohistochemistry of the biopsied lung of an IPF patient. **C:** Fibroblasts in the fibroblastic foci show strong positive staining for DDR1. **C** and **E:** Inflammatory cells in the IPF lesion are also stained positive for DDR1. **E:** The bronchoepithelial cells are negative for DDR1. In the non-IPF lung, only alveolar macrophages are stained weakly positive for DDR1 (**arrowheads**). **A** and **B:** H&E staining; **D** and **G:** nonspecific rabbit IgG; **E:** negative control for second antibody. Original magnifications: ×300 (**A**); ×500 (**B–H**).

sample from healthy volunteer) for 10 minutes. Subsequently, the cells were incubated with biotinylated anti-DDR1 antibodies[14] or fluorescein isothiocyanate-conjugated anti-α-SMA monoclonal antibodies (Sigma Chemical Co., St. Louis, MO) for 20 minutes at 4°C. After washing three times with PBS, the cells were incubated with streptavidin-PE (PharMingen) for 15 minutes at 4°C. Flow cytometry analysis was performed using a FACScan flow cytometer and CellQuest software (BD Biosciences, San Jose, CA).

Assay for Apoptosis

After five passages, 1×10^6 fibroblasts were seeded and incubated in the presence or absence of FasL (Calbiochem, La Jolla, CA), 50 μg/ml of type I collagen (Sigma-Aldrich, St. Louis, MO), CAPE (NF-κB inhibitor; Calbiochem), DDR1 agonistic antibodies, or control IgM.[14,17,25] To evaluate the effect of β1-integrin, another collagen receptor, we used monoclonal β1-integrin neutralizing antibodies (DE9, 10 μg/ml; Upstate Biotechnology, Lake Placid, NY), as previously described.[17,25] The apoptosis assay was performed by flow cytometry analysis using monoclonal antibodies for Annexin V-FITC and 7AAD (PharMingen), as described above. In all of the experiments, the apoptotic data were confirmed by terminal dUTP nick-end labeling assay, which was performed using a commercially available kit according to the manufacturer's instructions (TUNEL label mix; Roche Diagnostics Corp., Indianapolis, IN).

Western Blot Analysis

To detect the DDR1 isoforms, 1×10^7 fibroblasts after five passages or 1 mg of total lung tissue was lysed on ice for 20 minutes in 1 ml of lysis buffer containing 50 mmol/L HEPES, 150 mmol/L NaCl, 1% Triton X-100, 10% glycerol, and a cocktail of protease inhibitors (Roche). The lysates were centrifuged and 20 μl of the supernatant was collected. Subsequently, 20 μl of double-strength sample buffer (20% glycerol, 6% sodium dodecyl sulfate, and 10% 2-mercaptoethanol) was added to the supernatants. The samples were boiled for 10 minutes. The proteins were analyzed on 8% polyacrylamide gels by sodium dodecyl sulfate-polyacrylamide gel electrophoresis and transferred electrophoretically to nitrocellulose membranes at 150 mA for 1 hour using a semidry system. The membranes were incubated with rabbit IgGs that specifically recognize DDR1a,[16] DDR1b,[25] or both forms of DDR1 (Santa Cruz Biotechnology) or with anti-human actin monoclonal mouse IgG antibodies (Santa Cruz Biotechnology) followed by sheep anti-rabbit or mouse IgGs coupled with horseradish peroxidase (Amersham). The peroxidase activity was visualized by the enhanced chemiluminescence detection system (Amersham). The intensities of the DDR1 isoforms and actin were analyzed using the NIH Image Program (National Institutes of Health, Bethesda, MD), and the relative amount of each DDR1 isoform (DDR1 amount ratio) in each patient was then calculated.

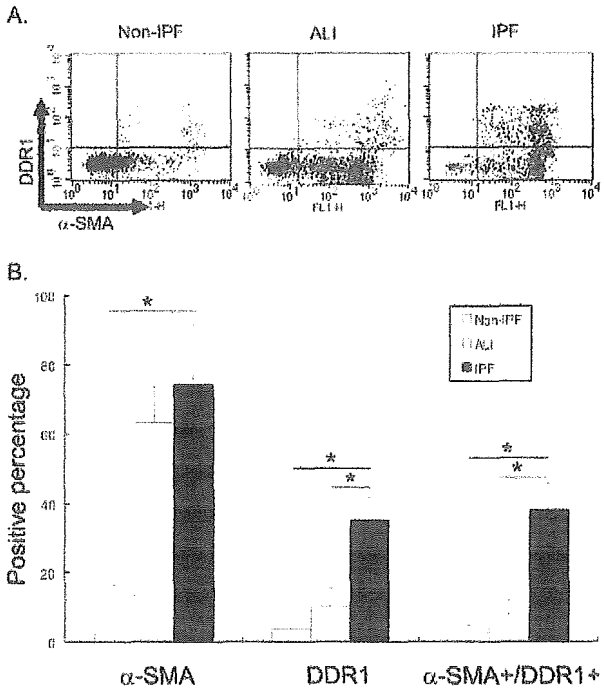

Figure 2. Flow cytometry analysis of cultured fibroblasts. The percentage of α-SMA-positive fibroblasts was significantly higher in the IPF patients than in the non-IPF patients. The percentage of α-SMA-positive fibroblasts was significantly higher in the ALI patients than in the non-IPF patients. The percentage of DDR1-positive fibroblasts was significantly higher in the IPF patients than in the ALI and non-IPF patients. The percentage of DDR1-positive/α-SMA-positive fibroblasts was significantly higher in the IPF patients than in the ALI and non-IPF patients. **A:** Representative data; **B:** comparison between seven different fibroblasts from seven different IPF patients, four different fibroblasts from four different ALI patients, and six different fibroblasts from six different non-IPF patients. $^*P < 0.01$, Bonferroni-Dunn test with one-way factorial analysis of variance.

To evaluate whether DDR1 activation by type I collagen or DDR1 agonistic antibodies induces autophosphorylation of DDR1 and DDR1 signal transduction, 1×10^7 fibroblasts after five passages were plated on dishes, serum-starved in RPMI 1640 containing 1% fetal calf serum for 10 hours, and subsequently activated with 50 μg/ml of type I collagen (Sigma) or DDR1 agonistic antibodies (513DDR1 ab).[17,25] The fibroblasts were then cultured for 1 hour. To evaluate the effect of monomeric collagen, 1×10^7 fibroblasts were seeded to type I collagen-coated dish (Iwaki Glass, Tokyo, Japan) and cultured for 1 hour after serum starvation. Cell lysates were prepared and DDR1 in the cell lysates was immunoprecipitated using anti-DDR1 antibodies (C-20; Santa Cruz Biotechnology) and recombinant protein G-agarose (Invitrogen, Gaithersburg, MD), as previously reported.[16,17,25] Additionally, tyrosine phosphorylation of DDR1 and Shc recruitment were analyzed by Western blotting by using mouse monoclonal anti-phosphotyrosine IgGs (4G10, Upstate Biotechnology) or mouse monoclonal anti-Shc antibodies (R&D Systems), followed by sheep anti-mouse IgGs coupled with horseradish peroxidase (Amersham). The peroxidase activity was visualized by the enhanced chemiluminescence detection system (Amersham).